

# Spin effects in thermoelectric properties of Al and P doped zigzag silicene nanoribbons

K. Zborecki<sup>1</sup>, R. Swirkowicz<sup>1</sup>, J. Barnaś<sup>2</sup>

<sup>1</sup>*Faculty of Physics, Warsaw University of Technology,  
ul. Koszykowa 75, 00-662 Warsaw, Poland and*

<sup>2</sup>*Faculty of Physics, Adam Mickiewicz University, ul. Umultowska 85, 61-614 Poznań, Poland  
and Institute of Molecular Physics, Polish Academy of Sciences, Smoluchowskiego 17, 60-179 Poznań, Poland*

(Dated: August 25, 2021)

Electric and thermoelectric properties of silicene nanoribbons doped with Al and P impurity atoms are investigated theoretically for both antiparallel and parallel orientations of the edge magnetic moments. In the former case, appropriately arranged impurities can lead to a net magnetic moment and thus also to spin thermoelectric effects. In the latter case, in turn, spin thermoelectric effects also occur in the absence of impurities. Numerical results based on *ab-initio* calculations show that the spin thermopower can be considerably enhanced by the impurities.

PACS numbers: xxx

## I. INTRODUCTION

Since the discovery of graphene, one can observe increasing interest in other two-dimensional honeycomb structures. One of such materials is silicene – a two-dimensional hexagonal lattice of silicon (Si) atoms. In contrast to graphene, silicene has a buckled atomic structure, where the two triangular sublattices are slightly displaced in opposite directions normal to the atomic plane. Band structure calculations show that silicene is a semimetal with zero energy gap and linear electronic spectrum near the  $K$  points of the Brillouine zone [1]. Similarly to graphene, electrons in the vicinity of the  $K$  points (Dirac points) behave like massless fermions. Apart from strictly two-dimensional crystals of silicene, also silicene nanoribbons have been fabricated recently [2–5].

Theoretical investigations of silicene have revealed a number of its interesting properties, like for instance the spin Hall effect induced by spin-orbit interaction [6] or an electrically tunable energy gap [7, 8]. The latter effect appears owing to the buckled atomic structure. Moreover, *ab-initio* numerical calculations have shown that two electrically-controlled gapped Dirac cones for nearly spin polarized states can exist when silicene is in a perpendicular electric field. Accordingly, an effective silicene-based spin filter has been proposed, where spin polarization of electric current can be switched with external electric field [9]. Since silicon plays a crucial role in the present-day electronics, integration of silicene into nanoelectronics seems to be more promising than that of graphene, and this possibility opens new perspectives for this novel material [10, 11]. Therefore, detailed description and understanding of physical properties of silicene is currently of great interest.

First-principle calculations based on the density functional theory (DFT) have shown that silicene surface is very reactive and can be easily functionalized [12]. This functionalization, in turn, can significantly change basic properties of silicene. Structural, electronic, magnetic and vibrational properties of silicene with adsorbed or

substituted atoms of various types have been extensively studied in recent years [12, 13]. The corresponding results show that the low-buckled lattice is stable in a wide range of doping [14]. Apart from this, both ad-atoms and substituted atoms induce characteristic modes in the phonon spectrum of silicene. A significant charge transfer between ad-atoms and silicene has also been reported [12].

Especially interesting are functionalization- and doping-induced modifications of transport properties. It has been shown that adsorption of alkali metals can transform silicene into a narrow gap semiconductor. On the other hand, by doping with transition-metal atoms, either semiconducting or metallic behavior can be obtained [13]. Furthermore, the band gap in silicene can be tuned when it is functionalized with hydrogen [15, 16]. As a result of semi-hydrogenation, i.e. hydrogenation from one side only, ferromagnetic ordering can be induced, and the system exhibits then semiconducting properties with a direct energy gap of the order of 1 eV [17]. It is worth noting that itinerant magnetism mediated by holes has been also predicted for AlSi monolayers as well as for AlSi armchair nanoribbons [18].

The electronic structure can be also modified by externally induced strain. For instance, it has been predicted that compressive (tensile) strain can move the Dirac points in silicene below (above) the Fermi level, so the system can behave like n-type (p-type) doped one [19]. Moreover, a sufficiently strong strain can reduce the thermal conductivity of silicene, as follows from non-equilibrium molecular dynamic simulations [20].

Apart from two-dimensional silicene crystals, also nanoribbons of armchair (aSiNRs) or zigzag (zSiNRs) type have been widely studied in view of potential applications in silicon-based electronics and spintronics devices. Similarly to graphene nanoribbons (GNRs), zSiNRs exhibit edge magnetic ordering. *Ab-initio* calculations for pristine zSiNRs show that antiferromagnetic (AFM) state, where magnetic moments of the two edges of a nanoribbon are antiparallel, corresponds to the lowest energy [21, 22]. Ferromagnetic (FM) ordering, in

which magnetic moments of the two edges are parallel, has a slightly higher energy and can be stable *eg* in an external magnetic field. In the FM state, zSiNRs have metallic transport properties, whereas in the AFM configuration a wide gap opens and zSiNRs display semiconducting behavior. Electronic, mechanical and magnetic properties of SiNRs have been studied recently by first principle methods [21–25]. In particular, investigations of electron transport properties of zSiNRs have revealed a giant magnetoresistance effect associated with transition from the FM to AFM configuration [24]. It has been also predicted that hydrogen-terminated zSiNRs in the presence of in-plane electrical field can behave like a half-metallic ferromagnet with spin polarization up to 99% [26]. When a local exchange field affects only one edge of zSiNRs, an energy gap can be opened in one spin channel, whereas the second spin channel remains gapless [27]. Spin gapless semiconductor behavior with 100% spin polarization has been also predicted for zSiNRs doped with B or N atoms in edge positions [28, 29]. On the other hand, in aSiNRs with B/N substitutions at the edges, semiconductor-metal transition due to formation of a half-filled impurity band near the Fermi level has been predicted [29]. Very recently, the interplay between bulk and edge states induced by Rashba spin-orbit coupling in zSiNRs has been investigated in the presence of electrical field [30]. It has been shown that the states with opposite velocities can open spin-dependent subgaps which remarkably influence spin polarized transport properties.

Thermoelectric properties of nanoscopic systems are currently of great interest due to the possibility of heat to electrical energy conversion at nanoscale, which is important for applications. Thermoelectric properties of aSiNRs and zSiNRs have been investigated by *ab-initio* methods based on DFT and non-equilibrium Green function formalism [21, 22]. It has been shown that thermopower of pristine zSiNRs in the low-energy AFM state can be considerably enhanced due to the presence of energy gaps. Moreover, the thermopower strongly depends on the magnetic configuration and a considerable magnetothermopower related to transition from the AFM to FM state can be observed [22]. In ferromagnetic systems, interplay between the spin effects and thermoelectric properties can lead to new spin related thermoelectric phenomena [31–34]. The most spectacular spin related thermoelectric effect is the spin thermopower (spin Seebeck effect) which is a spin analog of the conventional thermopower. A considerable spin thermopower has been predicted for pristine zSiNRs with FM ordering [22].

In the present paper we analyze electric and thermoelectric phenomena of zSiNRs doped with Al and P impurity atoms. It is shown that the spin thermopower can be considerably enhanced by impurities. In section 2 we present transmission function for zSiNRs. Thermoelectric properties in the AFM state are presented and discussed in section 3, while those in the FM state are considered in section 4. Summary and final conclusions

are in section 5.

## II. TRANSMISSION IN zSiNRs WITH Al AND P IMPURITY ATOMS

In this section we will present numerical results on electronic transmission in zSiNRs with impurities, obtained by *ab-initio* numerical calculations within the DFT Siesta code [35]. The nanoribbon edges were terminated with hydrogen atoms to remove the dangling bonds, and pristine zSiNRs as well as those with impurity atoms of Al or P type, localized at different positions with respect to the nanoribbon edges, were considered. The impurities were distributed periodically along the chain and localized (i) at one of the edges (PE configuration), (ii) at the nanoribbon center (PC configuration), and (iii) in the middle between the edge and central atoms of the nanoribbon (PM configuration). The elementary cell was adequately enlarged to include one impurity atom. The spin-resolved energy-dependent transmission  $T_\sigma(E)$  through nanoribbons was determined within the non-equilibrium Green function (NEGF) method as implemented in the Transiesta code [36]. The structures were optimized until atomic forces converged to 0.02 eV/Å. The atomic double-polarized basis (DZP) was used and the grid mesh cutoff was set equal to 200 Ry. The generalized gradient approximation (GGA) with Perdrew-Burke-Ernzerhof parameterization was applied for exchange-correlation part of the total energy functional [40]. The performed calculations, similarly to those presented in Refs [21, 22], show that antiferromagnetic (AFM) state, where magnetic moments at one edge are antiparallel to those at the other edge, is the most stable configuration (ground state) in pristine narrow zSiNRs. Ferromagnetic (FM) state, in which the edge moments are all parallel, corresponds to slightly higher energy. The energy difference between the two magnetic states is equal to 0.02 eV for pristine nanoribbon containing  $N=6$  zigzag chains. Thus, magnetic configuration of pristine zSiNRs can be easily changed from the AFM state to the FM one, for instance by an external magnetic field.

### A. Low energy state

In Fig. 1 we show spin density for zSiNRs in the ground state (referred to in the following as the low energy state) for the three different impurity configurations, i.e. PE, PC and PM ones. In the presence of non-magnetic impurity atoms (Al, P), magnetic moments at the two nanoribbon edges do not fully compensate each other. Moreover, some small moments are also localized on inner atoms (see Fig. 1). As a result, small net magnetization can be observed in the low energy state. Our calculations also show, that when the impurity concentration at the edge (PE configuration) increases, the low-energy

state becomes ferromagnetic, with magnetic moments located only at the impurity-free edge of the nanoribbon (see Fig. 2). This happens when the distance between the edge impurity atoms is smaller than 19 Å, which is in agreement with Refs [28, 29]. Thus, the low-energy state is antiferromagnetic for pristine nanoribbons, generally ferrimagnetic in nanoribbons with impurities, and ferromagnetic for impurities located at one edge and of a sufficiently large concentration. Since smaller impurity concentrations are easier to be achieved experimentally, we have performed calculations for zSiNRs with longer distance between the impurities. More specifically, the distance is equal to the size of the elementary cell shown in Fig.1. Note, Fig.2 displays more elementary cells, as the distance between impurities is there smaller than in Fig. 1. To be more specific, the elementary cell shown in Fig. 1 is the system through which transmission is calculated, while the left and right semi-infinite parts of the nanoribbon are treated as external electrodes.

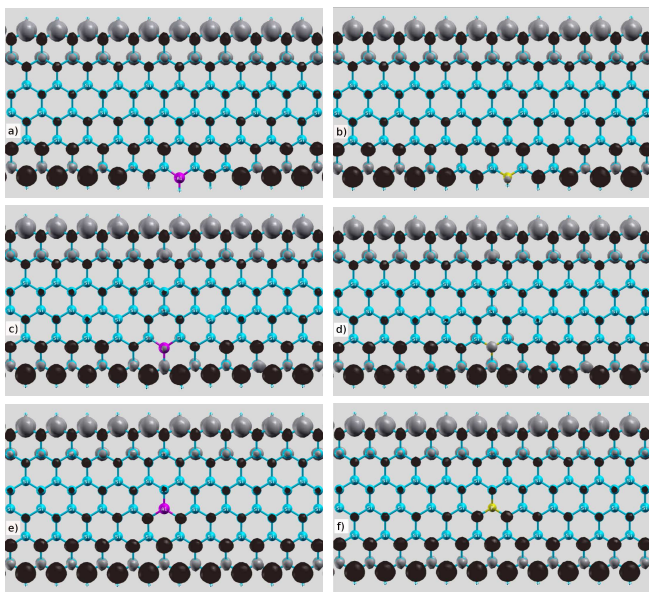


FIG. 1: (Color online) Spin density in the low energy state, calculated within GGA approximation for zSiNRs with  $N = 6$  for Al (left panel) and P (right panel) impurities in the PE (a,b), PM (c,d) and PC (e,f) configurations. Black and gray dots represent magnetic moments of opposite directions.

Transmission function  $T_\sigma(E)$  corresponding to the nanoribbons shown in Fig. 1 is presented in Fig. 3 for both spin orientations. The transmission is shown there as a function of energy measured from the corresponding Fermi energy  $E_F$ . One can note that the energy gap at the Fermi level, which exists in pristine zSiNRs in the AFM state (inset to Fig. 3a), survives also in the presence of impurity atoms. However, transmission depends now on the spin orientation because magnetic moments of the two edges do not fully compensate each other in the presence of impurities. Moreover,  $T_\sigma(E)$  depends on the type

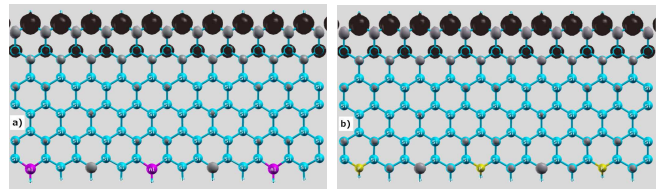


FIG. 2: (Color online) Spin density in the one-edge FM state, calculated within GGA approximation for zSiNRs with  $N = 6$  for Al (left) and P (right) impurities in the PE configuration. Note, the density of impurity atoms is here larger than in Fig. 1. Meaning of the black and gray dots same as in Fig. 1.

and position of impurities. The transmission is strongly modified near the edges of the energy gap. The impurity atoms can lead to states localized in the gap, which give narrow peaks in the transmission function – especially well visible for Al atoms in the PM configuration (below the Fermi level) and in the PC configuration of P impurities (above the Fermi level). Apart from the wide gap near the Fermi energy  $E_F$ , additional gaps appear in the spectrum at other energies. A wide gap opens above the Fermi level in the spin-up channel for Al impurities localized at the nanoribbon edge, and a similar gap appears below the Fermi level in the spin-down channel for P impurities (Fig. 3). It is interesting to note that spin-down electrons in the former case and spin-up holes in the latter case are less influenced by the impurities, so the corresponding gaps are much narrower. The transmission exhibits also a number of antiresonance dips – mainly for higher values of  $|E - E_F|$ . In the presence of impurity atoms, quantum interference can lead to Fano antiresonances. Especially interesting results are obtained for the PC impurity configuration, where typical and well defined Fano antiresonances in nanoribbons with P impurity atoms appear in the transmission in the vicinity of  $E - E_F = 0.5$  eV (Fig. 3f). Due to the destructive interference, a relatively wide gap appears in this energy region, with transmission close to zero. On the other hand, in nanoribbons with Al impurity atoms in the PC configuration, the Fano antiresonance can be observed near  $E - E_F \approx -0.5$  eV as well as for  $E - E_F \approx 0.4$  eV. The interference effects are more pronounced for spin-up carriers in nanoribbons with P impurities, and spin-down carriers in nanoribbons with Al impurities, as considerable magnetic moments are then localized on nearby Si atoms. Well defined Fano antiresonances can be also visible for Al impurities in the PM configuration (inset to Fig. 3c)

## B. Ferromagnetic state

Consider now nanoribbons which display ferromagnetic ordering (FM state) in the absence as well as presence of impurities. As already mentioned above, energy

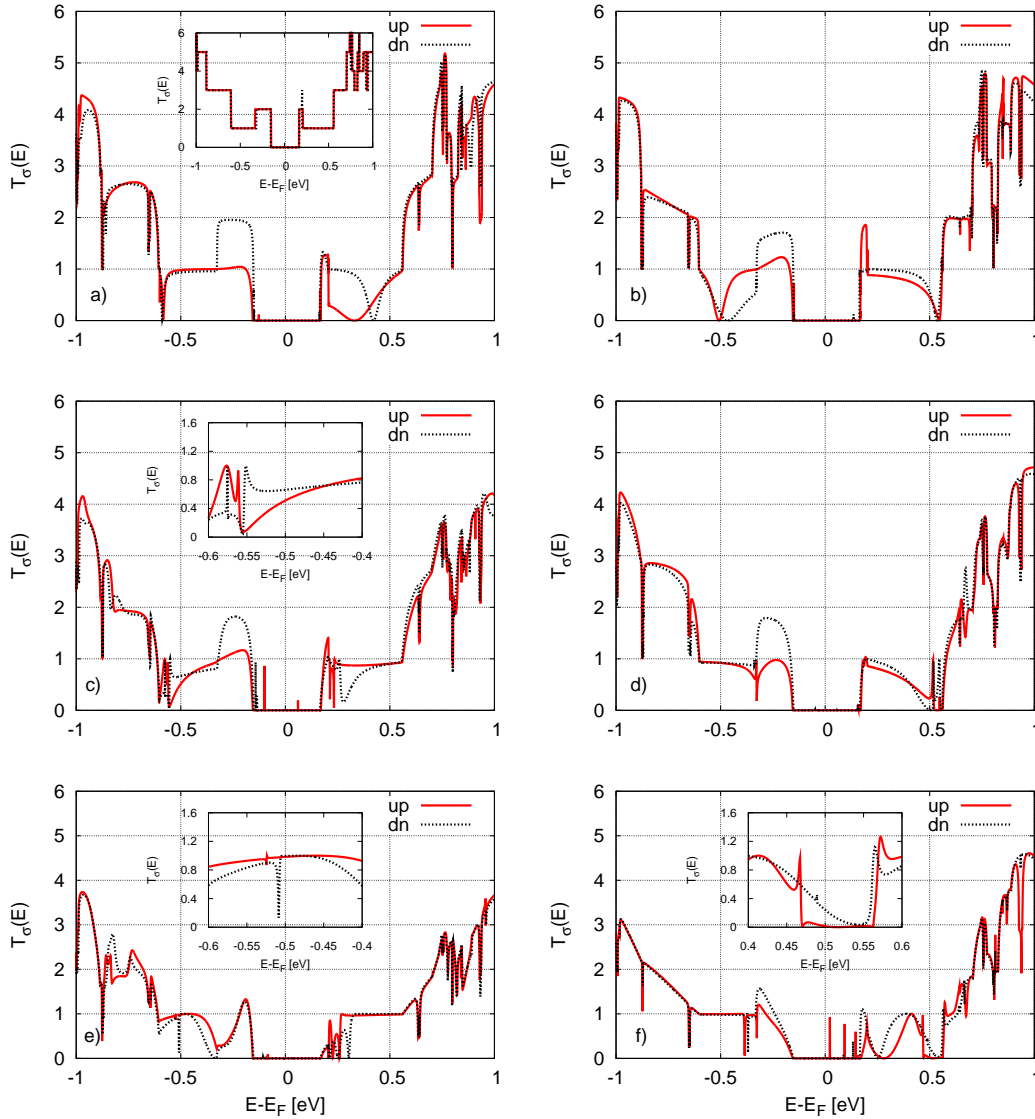


FIG. 3: (Color online) Spin-dependent transmission in zSiNR ( $N=6$ ) in the low-energy state as a function of energy, calculated within the GGA approximation for pristine nanoribbon (inset to a) and for Al (left panel) and P (right panel) impurities in the PE (a,b), PM (c,d), and PC (e,f) configurations, respectively. Insets to Figs. c,e,f show transmission in a narrow energy range, where the Fano antiresonances are well resolved.

of such a state is only slightly higher than that of the above discussed low-energy (ground) state. Thus, the FM state can be stabilized by an external magnetic field or by other methods. Spin density for the three different configurations of impurity atoms is presented in Fig. 4. Note, magnetic moments localized at the two edges are not equal in the presence of impurities.

The corresponding spin-resolved transmission function is shown in Fig. 5. Pristine ferromagnetic zSiNRs exhibits typical metallic behavior with a constant transmission in the vicinity of the Fermi level, see the inset to Fig. 5a. In the presence of impurity atoms localized at one of the edges, the metallic character, with almost

constant transmission, is preserved for energies very close to  $E_F$ . For both kinds of impurities, transmission shows a narrow dip below the Fermi level for spin-up electrons, and similar dip above the Fermi level for spin-down electrons, see Figs 5a,b. Additional and more pronounced dips appear for energies close to  $\pm 0.5$  eV. These dips appear for both spin orientations, but are slightly separated in energy. It is also interesting to note that in the case of P impurities a wider dip corresponds to holes ( $E - E_F < 0$ ), whereas for Al impurities the well defined and wide dip appears for electrons ( $E - E_F > 0$ ).

When the impurities are shifted towards the center of the nanoribbon, some important modifications in the

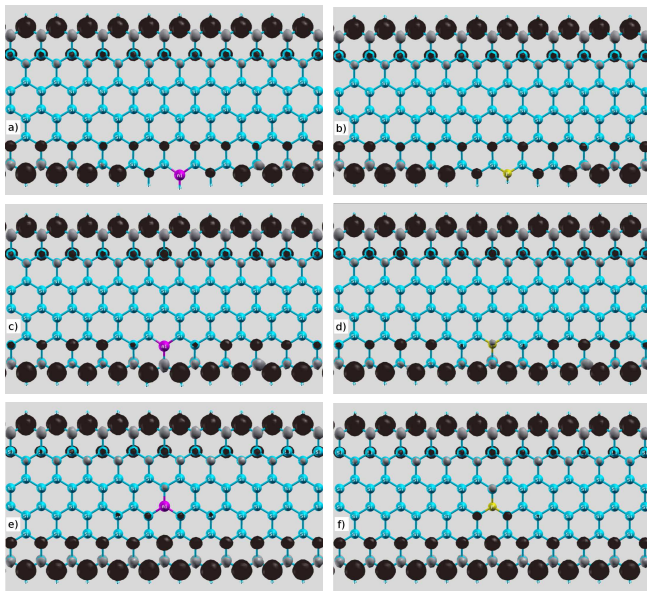


FIG. 4: (Color online) Spin density in the FM state, calculated within GGA approximation for zSiNRs ( $N=6$ ) for Al (left panel) and P (right panel) impurities in the PE (a,b), PM (c,d) and PC (e,f) configurations, respectively. Meaning of the black and gray dots same as in Fig. 1.

transmission function appear. Interesting behavior can be noticed for the PM impurity configuration (Figs 5c,d). One spin channel (spin-down for Al and spin-up for P) remains then conductive (metallic) in the close vicinity of the Fermi level, whereas the second channel becomes semiconducting due to a wide dip in the transmission at the Fermi level. One may expect that the dip appears due to pronounced Fano antiresonance. This behavior significantly changes in the PC configuration, with the impurity atoms localized in the center of the nanoribbon (Figs. 5e,f). Both spin channels are then conductive in the close vicinity of the Fermi level and metallic character of the system is recovered. However, pronounced dips in the transmission spectrum appear for electrons (P impurities) and holes (Al impurities). It is worth to note that the Fano antiresonances appear for energies well above or below the Fermi level. In particular, for energies close to 0.5 eV positive interference effects in nanoribbons with P defects lead to a very well defined peak, which is followed by a wide gap resulting from destructive interference, see the inset to Fig. 5f. Since the transmission is strongly spin dependent, the resonances for spin-up and spin-down channels are well separated. For Al impurities, narrow Fano dips appear for both spin channels, but now the effect can be observed for energies below the Fermi level and corresponds to the holes. Thus, changing the impurity type one can observe quantum interference effects for electrons or holes.

Transport properties of nanoribbons with (and without) defects are fully determined by the transmission

function. Thus, having found  $T_\sigma(E)$  one can determine not only electric conductance, but also thermoelectric parameters. This will be presented in the following sections, and we begin with the low energy (ground) state.

### III. ELECTRIC AND THERMOELECTRIC PROPERTIES OF zSiNRs IN THE LOW ENERGY STATE

In the low-energy state of pristine zSiNRs, the two spin channels are equivalent. However, since a nonzero net magnetization generally appears in the presence of impurities, these two channels are then no longer equivalent. When the spin channels are mixed in the nanoribbon on a distance comparable to the system length, no spin thermopower can be observed and only conventional thermoelectric phenomena can occur. We will consider first this limit.

In the linear response regime, the electric  $I$  and heat  $I_Q$  currents flowing through the system from left to right when the difference in electrical potential and temperature of the left and right electrodes is  $\Delta V$  and  $\Delta T$ , respectively, can be written in the matrix form as [22]

$$\begin{pmatrix} I \\ I_Q \end{pmatrix} = \begin{pmatrix} e^2 L_0 & \frac{e}{T} L_1 \\ e L_1 & \frac{1}{T} L_2 \end{pmatrix} \begin{pmatrix} \Delta V \\ \Delta T \end{pmatrix}, \quad (1)$$

where  $e$  is the electron charge, while  $L_n = \sum_\sigma L_{n\sigma}$ , with  $L_{n\sigma} = -\frac{1}{h} \int dE T_\sigma(E) (E - \mu)^n \frac{\partial f}{\partial E}$  for  $n = 0, 1, 2$ . Here,  $T_\sigma(E)$  is the spin-dependent transmission function for the system and  $f(E - \mu)$  is the Fermi-Dirac distribution function corresponding to the chemical potential  $\mu$  and temperature  $T$ .

Basic transport coefficients can be expressed in terms of  $L_n$ . The electrical conductance  $G$  is given by the formula  $G = e^2 L_0$ , whereas the electronic contribution to the thermal conductance,  $\kappa_e$ , is equal to

$$\kappa_e = \frac{1}{T} \left( L_2 - \frac{L_1^2}{L_0} \right). \quad (2)$$

In turn, the thermopower,  $S = -\Delta V / \Delta T$ , is expressed by the formula

$$S = -\frac{L_1}{|e| T L_0}. \quad (3)$$

In the linear response regime considered in this paper, transport properties are determined by electronic states near the Fermi level. In reality the chemical potential in nanoribbons (measured from the Fermi energy  $E_F$ ) can be easily varied with an external gate voltage. This technique offers a unique possibility to realize various positions of the Fermi level in a single sample. Alternatively, the chemical potential can be moved down or up by p-type or n-type doping, which results in  $\mu < 0$  and  $\mu > 0$ , respectively. We assume that this doping does not influence transmission functions calculated above, and the

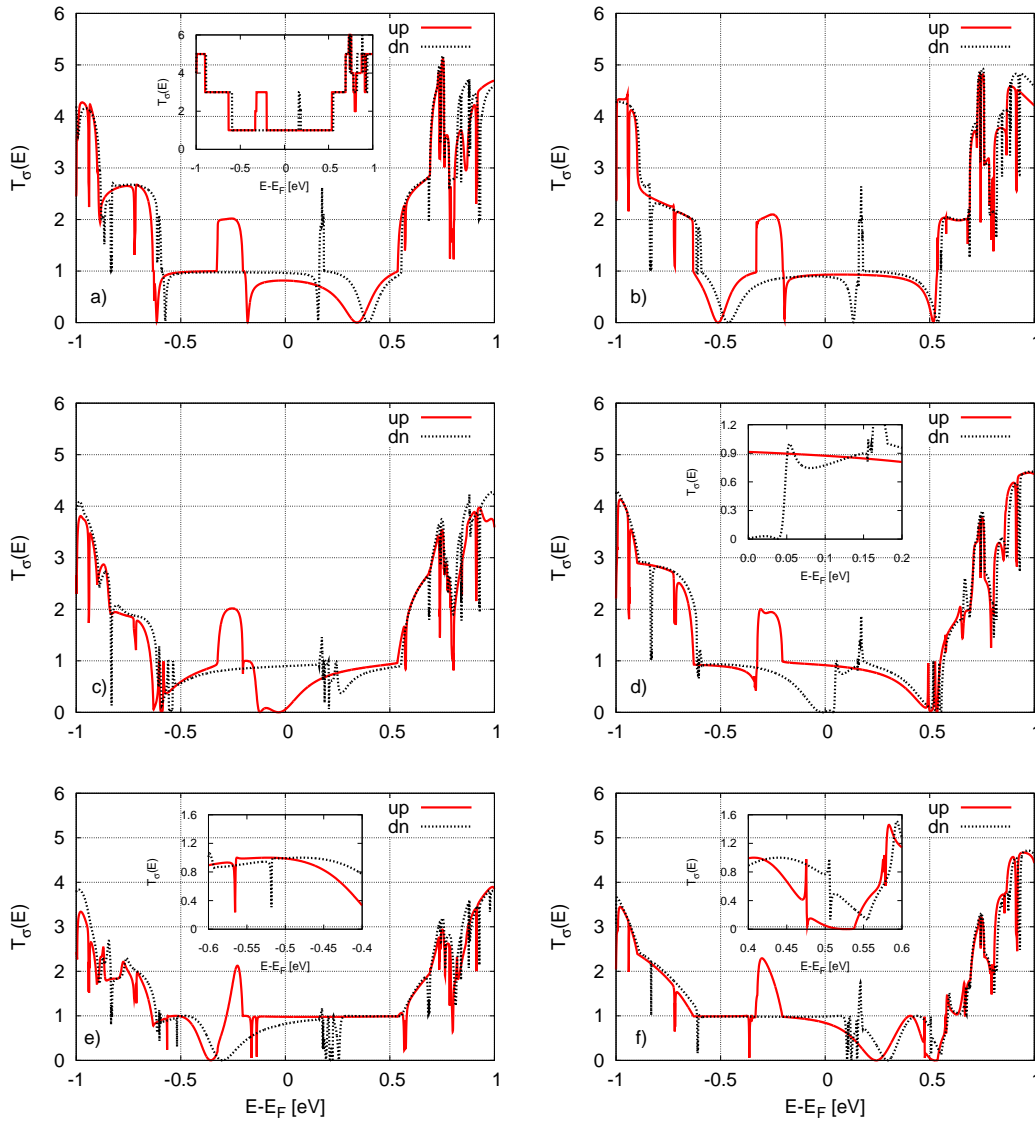


FIG. 5: (Color online) Spin-dependent transmission for zSiNRs ( $N=6$ ) in the FM state as a function of energy, calculated within the GGA approximation for pristine ribbon (inset to a) and for Al (left panel) and P (right panel) impurities in the PE (a,b), PM (c,d), PC (e,f) configurations. Insets to e and f show the transmission in a narrow energy range, where the Fano antiresonances are well resolved.

donors/acceptors are different from the substituted P and Al atoms. Significant changes in the chemical potential can be caused by a substrate, too.

Using the transmission functions through the system (central part of the nanoribbon) determined in the previous section for the low-energy state of pristine and doped zSiNRs, one can calculate the electrical conductance  $G$  and electronic term in the thermal conductance,  $\kappa_e$ , as well as the thermopower  $S$ . The results are presented in Fig. 6 as a function of the chemical potential  $\mu$  for Al and P impurities, and for all the three impurity configurations (PE, PM and PC ones). For comparison we also show there the results for pristine nanoribbons. For the

temperature  $T = 90$  K assumed in Fig. 6, the energy gap in the vicinity of  $\mu = 0$  is well resolved in the electric and in the thermal conductance. For pristine zSiNRs, both  $G$  and  $\kappa_e$  rapidly increase near the gap edges reaching maximum, and then become reduced with a further increase in  $|\mu|$ . For higher values of  $|\mu|$ , the conductances increase again. In the presence of impurity atoms, both  $G$  and  $\kappa_e$  are substantially reduced in the whole region of the chemical potential, as shown in Figs. 6a,b for  $G$  and Figs. 6e,f for  $\kappa_e$ . When the impurities are localized at the nanoribbon edge (PE configuration), the conductance shape is similar to that in pristine system, especially near the gap, though the conductance is reduced.

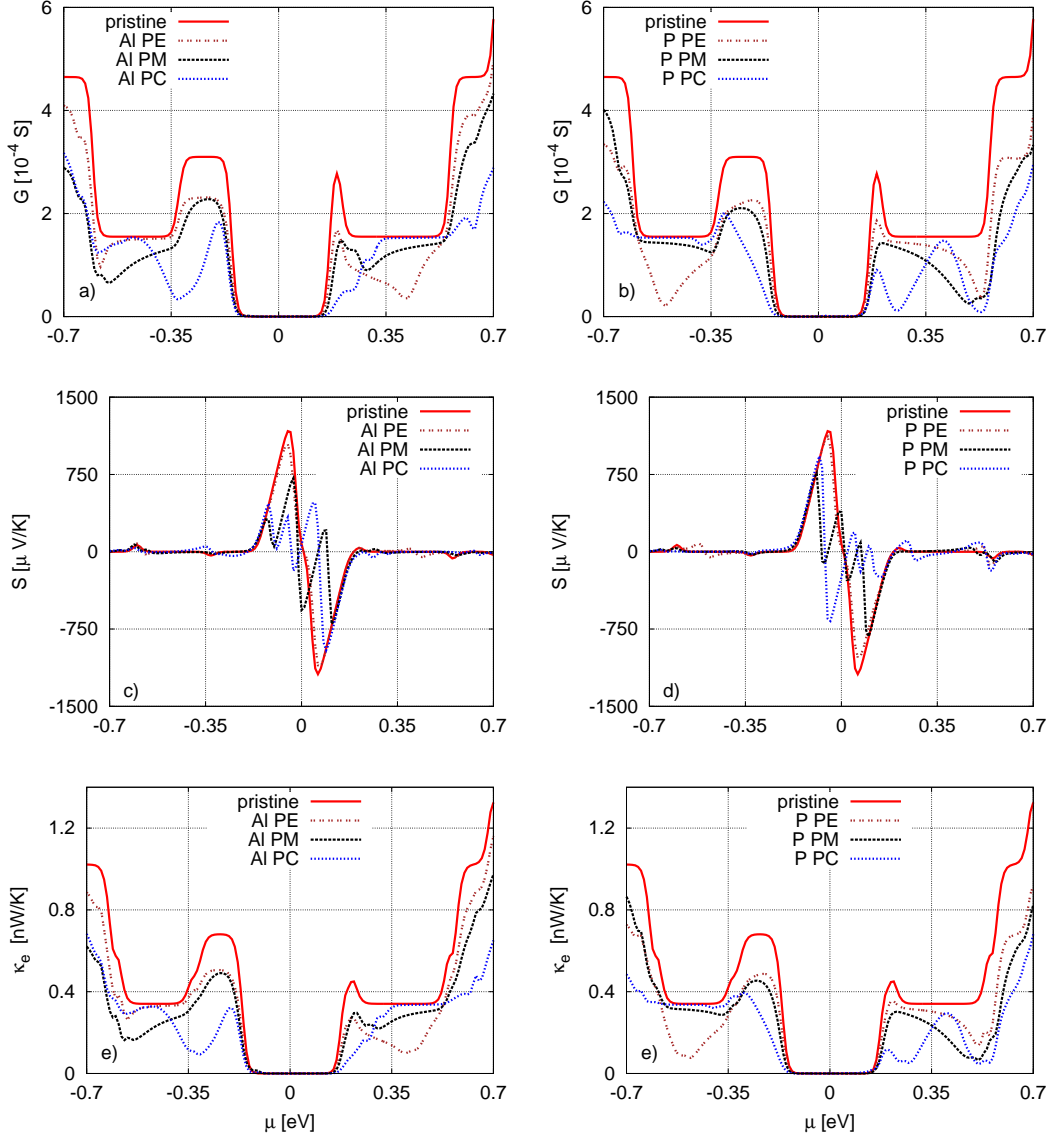


FIG. 6: (Color online) Conductance (a,b), thermopower  $S$  (c,d) and electronic term in the thermal conductance  $\kappa_e$  (e,f) as a function of the chemical potential  $\mu$  for zSiNRs in the low-energy state with Al (left panel) and P (right panel) impurities, calculated for  $T = 90$  K,  $N=6$ , and the three considered impurity configurations.

Moreover, a pronounced dip appears in the region of negative  $\mu$  ( $\mu \approx -0.5$  eV) for P impurities and for positive  $\mu$  ( $\mu \approx 0.4$  eV) for Al impurities. Much stronger modifications occur in the PC configuration, with defects localized in the nanoribbon center. The conductances  $G$  and  $\kappa_e$  are then remarkably reduced near the gap edges, especially for negative  $\mu$  for P impurities and positive  $\mu$  for Al impurities.

The thermopower  $S$  of pristine nanoribbon is considerably enhanced inside the main gap in the spectrum (around  $E_F$ ), with maxima (positive and negative) at the chemical potentials of several  $kT$  from the left and right gap edges. The maxima appear when either par-

ticle transport (for negative  $\mu$ ) or hole transport (for positive  $\mu$ ) becomes suppressed, as discussed in details in Ref. 22. A large value of  $|S|$ , exceeding 1mV/K, results from rapid increase in transmission near the gap edges. Similar enhancement of the thermopower also appears in the presence of impurities in the PE configuration. However, for nanoribbons with impurities in the PC configuration, the thermopower is considerably reduced since transmission near the gap edges is diminished and changes more smoothly. Moreover, a kind of damped oscillations of  $S$  inside the gap can be observed, which follow from states localized in the gap. It is interesting to note that the global maximum of the thermopower in

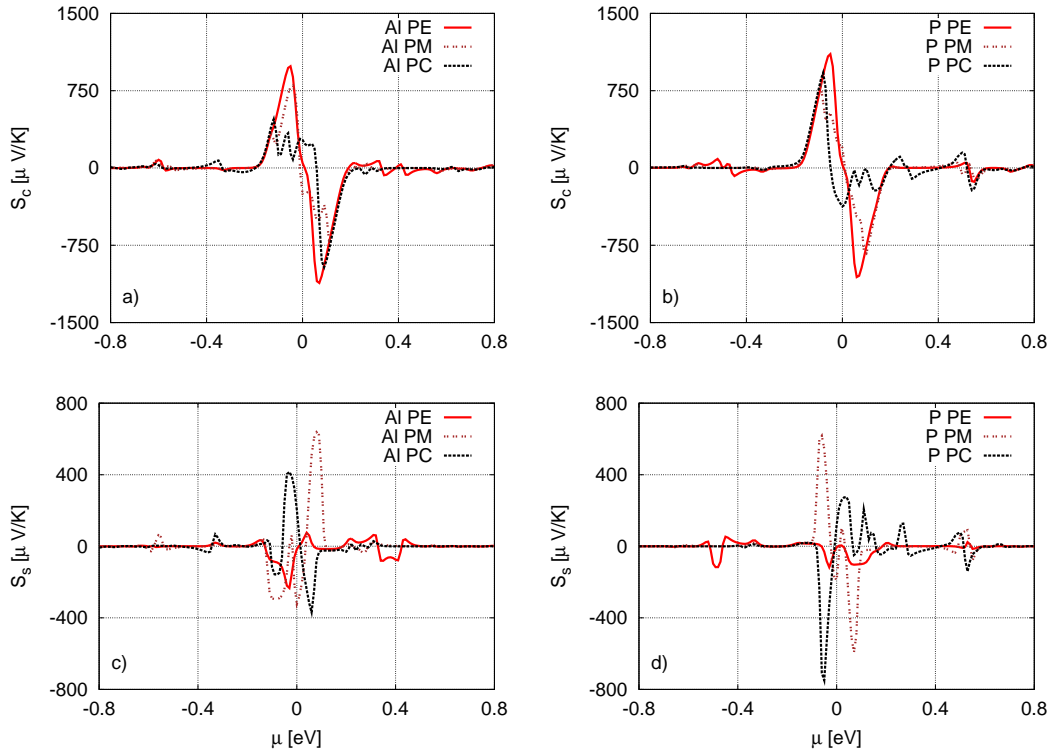


FIG. 7: (Color online) Charge and spin thermopowers as a function of the chemical potential  $\mu$ , calculated for the low-energy state of zSiNRs with Al (left panel) and P (right panel) impurities in the three (PE, PM, and PC) configurations, and for  $T=90\text{K}$  and  $N=6$ .

the presence of P defects in the PC configuration is positive and appears near the left edge of the gap (negative  $\mu$ ), whereas such a global maximum in the presence of Al impurities is negative and appears near the right edge of the gap (positive  $\mu$ ). In the presence of impurities, the thermopower is also enhanced for higher values of  $|\mu|$ . This enhancement, however, is less pronounced than that for  $\mu$  inside the main gap.

Situation may change when the spin channels are either not mixed in the nanoribbon, or they are mixed on a scale much longer than the system's length. The spin effects in thermoelectric properties become then important. The electrical conductance  $G_\sigma$  of the spin- $\sigma$  channel is equal to  $e^2 L_{0\sigma}$ ,  $G_\sigma = e^2 L_{0\sigma}$ , whereas the total electronic contribution to the thermal conductance,  $\kappa_e$ , is given by the formula

$$\kappa_e = \frac{1}{T} \sum_{\sigma} \left( L_{2\sigma} - \frac{L_{1\sigma}^2}{L_{0\sigma}} \right). \quad (4)$$

Since the two spin channels are not mixed and spin accumulation is important, one can introduce spin-dependent thermopower,  $S_\sigma = -\Delta V_\sigma / \Delta T = -L_{1\sigma} / |e| T L_{0\sigma}$ , which corresponds to the spin-dependent voltage generated by a temperature gradient [22, 34]. The conventional (charge) and spin thermopowers can be then written as  $S_c = \frac{1}{2}(S_\uparrow + S_\downarrow)$  and  $S_s = \frac{1}{2}(S_\uparrow - S_\downarrow)$ , respectively.

We assume the transmission through the system (central part of the nanoribbon) is the same for nanoribbons with and without spin relaxation. In Fig. 7 we show both charge and spin thermopowers as a function of chemical potential for all the three considered localizations of the Al and P impurity atoms. It is interesting to note, that the spin thermopower is relatively large due to a significant spin dependence of the transmission function in the presence of impurities and for the assumed distance between the impurity atoms. The impurity-induced spin thermopower depends on the location of the impurities and is especially large in the PC and PM configurations. When the impurities are located at one of the edges, the spin thermopower is remarkably smaller. Note, the conventional (charge) thermopower is also modified as follows from comparison of the results shown in Fig. 7 with the corresponding ones in Fig. 6. This modification appears due to impurity-induced spin dependence of the transmission function. Some modifications induced by impurities appear also in other transport coefficients, for instance in the electronic contribution to the heat conductance, which however are not presented here explicitly.

#### IV. ELECTRIC AND THERMOELECTRIC PROPERTIES OF $z$ SiNRs IN THE FERROMAGNETIC STATE

By applying an external magnetic field one can stabilize the ferromagnetic (FM) configuration of  $z$ SiNRs. This configuration can be also stabilized by exchange coupling to a ferromagnetic substrate or to ferromagnetic contacts. Due to a significant magnetic moment in the FM state, transmission function of a nanoribbon is strongly spin-dependent.

Using the spin-resolved transmission  $T_\sigma(E)$  determined in Sec. 2B for the ferromagnetic state of pristine nanoribbons as well as of nanoribbons with impurities, we investigate now the spin-polarized transport phenomena. Spin-resolved electrical conductance  $G_\sigma$  as a function of chemical potential  $\mu$  is presented in Fig. 8 for different positions of the Al and P impurity atoms, whereas the thermal conductance  $\kappa_e$  is depicted in Fig. 9. Pristine ferromagnetic nanoribbons as well as those with impurities in the PE configuration show metallic character. The conductance  $G_\sigma$  is then constant in a close vicinity of  $\mu = 0$  and it is practically the same for both spin channels for P impurities, and weakly depends on spin for Al impurities. Strong modifications appear for higher values of  $|\mu|$ , where due to a pronounced dip in the transmission, one spin channel becomes weakly conductive and a considerable polarization  $P$ , defined as  $P = \frac{G_\uparrow - G_\downarrow}{G_\uparrow + G_\downarrow} \times 100\%$ , can be observed. It is worth to note that the presence of P atoms at one of the edges leads to a considerable polarization (up to 90%) in a narrow region of negative  $\mu$ , whereas for Al impurities a large polarization can be obtained for positive  $\mu$ . For other values of chemical potential, the spin polarization is much smaller, though in narrow regions of  $\mu$  it can achieve even 50%. Interesting results are obtained for the PM impurity configuration, where one spin channel – spin up for Al and spin down for P impurities – becomes nonconductive in a close vicinity of  $\mu=0$ , whereas the second channel exhibits metallic character. The system behaves thus like a half-metallic ferromagnet with practically 100% polarization. Such a behavior can be important for potential applications of doped silicene nanoribbons in spintronic devices. Relatively high polarization can be also obtained for PC configuration, but in a narrow region of negative  $\mu$  for Al impurity and positive  $\mu$  for P impurities. Moreover, the conductance of a nanoribbon with central P impurities exhibits pronounced spin-dependent dips in the energy region close to  $\mu=0.55$  eV, resulting from the well-defined spin-dependent Fano antiresonance in the transmission. On the other hand, narrow spin-dependent Fano dips, which occur in transmission well below the Fermi energy for Al impurities in the PC configuration do not give visible modifications of the conductance.

When spin mixing takes place on a distance comparable to the systems's length, then only conventional thermoelectric effects can be observed. In turn, when spin relaxation processes are absent, spin effects become rel-

evant. Below we present numerical results just for this particular case.

Thermal conductance  $\kappa_e$  of the ferromagnetic nanoribbons with impurities is considerably reduced as compared to that of the pristine ones. Bearing in mind thermoelectric properties, it can be important that  $\kappa_e$  is remarkably reduced in the vicinity of  $\mu = 0$  for the PM impurity configuration due to the gap occurring for one spin channel. Substantial reduction of  $\kappa_e$  is also obtained for negative and positive  $\mu$  for one of the PE or PC configurations (Fig. 9). The thermal conductance is additionally reduced for P impurities in the PC configuration due to the well-defined Fano antiresonance for chemical potentials close to 0.55 eV.

The influence of impurity atoms on the charge and spin thermopowers is presented in Fig. 10. For comparison, the thermopower of a pristine nanoribbon is also depicted there. As a general rule one can state that impurity atoms (Al, P) strongly enhance both charge and spin thermopowers. However, the modifications depend on the position and type of the impurities. Very remarkable changes can be observed for impurity atoms in the PM configuration, in which – due to appearance of energy gap in one of the spin channels – the charge and spin thermopowers are strongly enhanced in a close vicinity of  $\mu = 0$ . It should be also noticed that the main contribution to  $S_c$  and  $S_s$  in the case of Al atoms comes from the majority (spin-up) carriers, as this spin channel becomes nonconductive in the presence of Al impurities. On the other hand, in nanoribbons with P impurities, both  $S_c$  and  $S_s$  show different signs, which indicates that the main contribution corresponds to non-conductive spin-down channel. Totally different results are obtained for pristine nanoribbons.

Since pristine ferromagnetic nanoribbons exhibit metallic character for both spin directions, the transmission is constant in the region of small  $|\mu|$  and both  $S_c$  and  $S_s$  are negligibly small in this region of chemical potential. Similar behavior can be observed for nanoribbons with impurities in the PE and PC configurations, where both thermopowers are practically equal to zero for small values of  $|\mu|$ . However, a considerable enhancement of  $S_c$  and  $S_s$  is then obtained for higher values of  $|\mu|$ , where pronounced dips occur in transmission function. High value of  $|S|$  in the vicinity of  $\mu \approx 0.55$  eV for P impurities can be related to the Fano antiresonance, and thus to rapid changes in transmission function (Fig. 3). As the Fano effect in FM state is strongly spin dependent, the remarkable spin thermopower close to 0.15 mV/K can be observed in this situation. Strongly enhanced charge and spin thermopowers are also obtained for P impurities localized near the edges, but they appear for negative  $\mu$ . The Al atoms in the PE and PC configurations also lead to quite remarkable modifications. It should be noticed that the edge position of Al atoms leads to considerable enhancement of  $|S|$  for positive  $\mu$ , whereas impurities localized in the center enhance  $|S|$  for negative values of chemical potential. The opposite relations are found

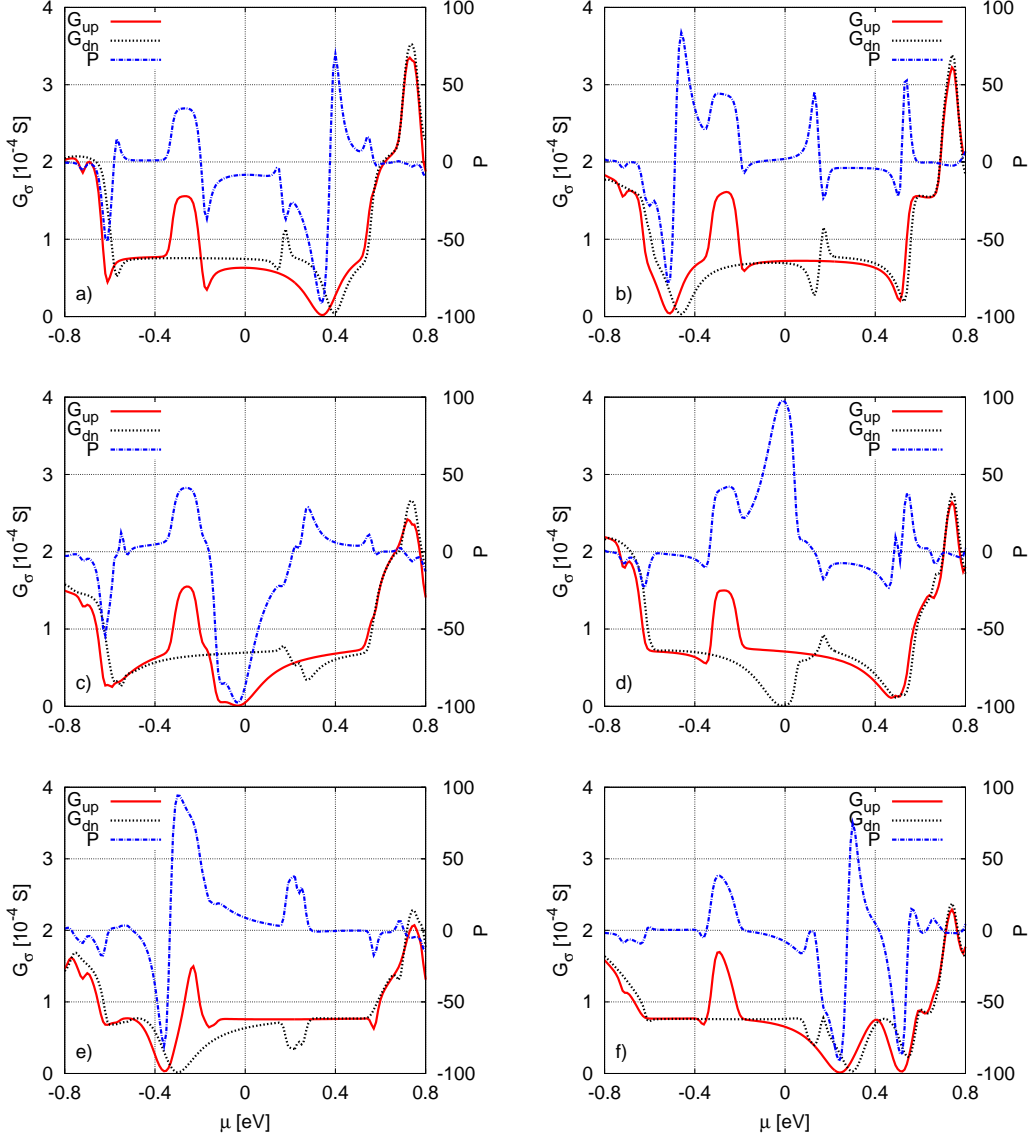


FIG. 8: (Color online) Spin-dependent conductance  $G_\sigma$  and polarization  $P$  as a function of chemical potential  $\mu$ , calculated for the FM state of ZSiNRs with Al (left panel) and P (right panel) impurity atoms in the configurations PE (a,b), PM (c,d), and PC (e,f). The other parameters are  $T = 90$ K, and  $N = 6$ .

for P impurities, where  $|S|$  is enlarged for the edge configuration in the region of negative  $\mu$  but for PC configuration the enhancement is for positive  $\mu$ . All this shows that type of impurities (Al or P) and their localization in the nanoribbons play an important role.

## V. SUMMARY AND CONCLUSIONS

We have considered transport and thermoelectric effects in silicene nanoribbons with Al and P impurity atoms. Using *ab-initio* calculations we have determined

transmission function through a nanoribbon. Using the calculated transmission we have determined thermoelectric coefficients in the linear response regime, like Seebeck and spin Seebeck parameters as well as the electronic contribution to the heat conductance. The results have been presented for two different situations corresponding to presence and absence of short-range spin mixing in the nanoribbons. The calculations have been performed for both antiparallel (AFM, low energy) and parallel (FM) configurations of the edge magnetic moments.

The key objective was to determine the role of impurity atoms located in various positions with respect to the nanoribbon center. Numerical results clearly show

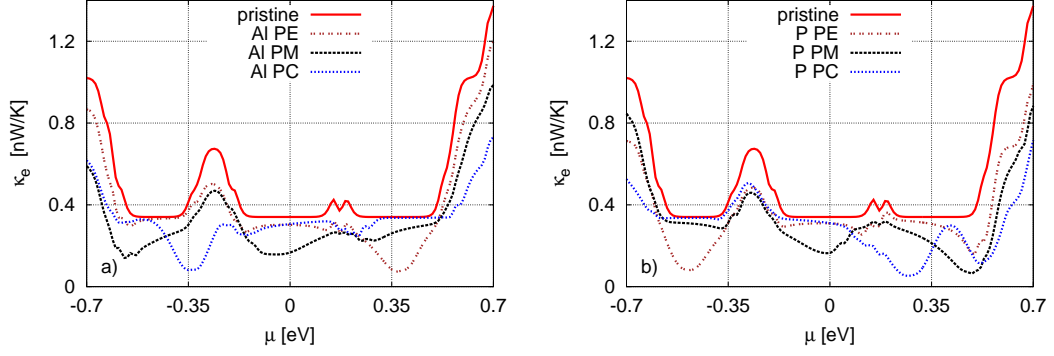


FIG. 9: (Color online) Electronic term in the thermal conductance,  $\kappa_e$ , as a function of chemical potential  $\mu$  in the FM state of zSiNRs for Al (a) and P (b) impurities, and for  $T = 90\text{K}$  and  $N = 6$ .

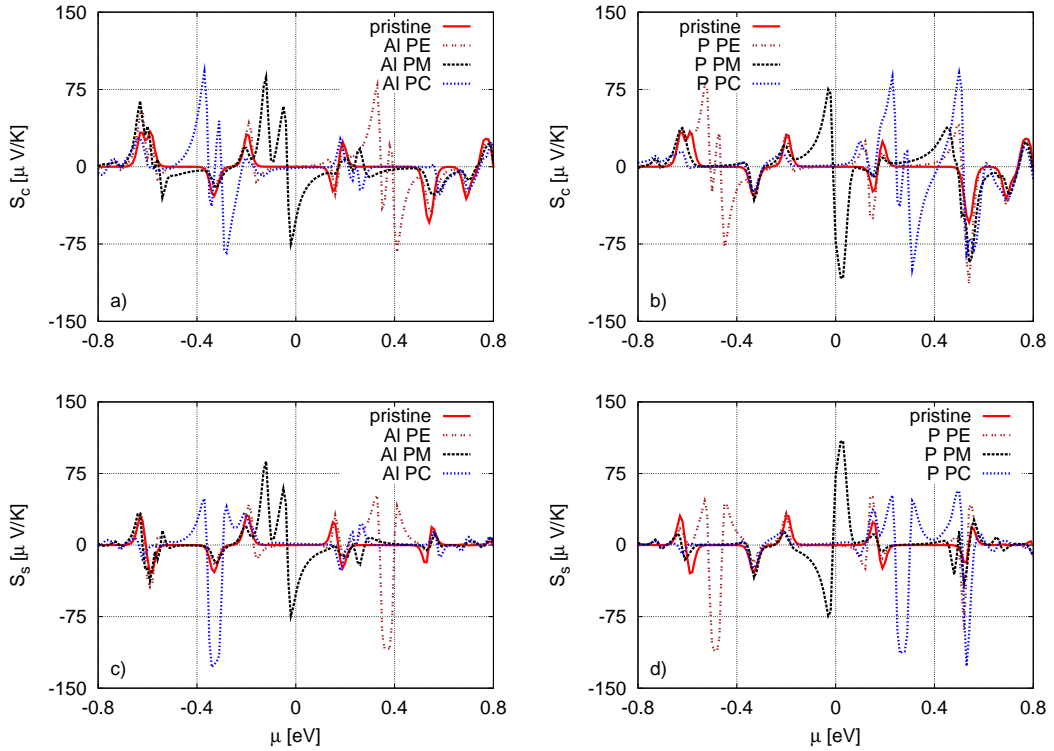


FIG. 10: (Color online) Charge  $S_c$  and spin  $S_s$  thermopower as a function of chemical potential  $\mu$  calculated for the FM state for zSiNRs with Al (a,c) and P (b,d) impurities, and for  $T = 90\text{K}$  and  $N = 6$ .

that the Al and P impurity atoms significantly modify the transmission function, and thus also the thermoelectric coefficients. More specifically, the Seebeck and spin Seebeck coefficients are remarkably enhanced by the impurities. This enhancement depends on position of the impurities. We have considered three different impurity configurations – PE (impurities at one of the edges), PC (impurities in the center of the nanoribbon), and PM (impurities between the edge and center of the nanoribbon).

## Acknowledgments

This work was supported by the National Science Center in Poland as the Project No. DEC-2012/04/A/ST3/00372. Numerical calculations were performed at the Interdisciplinary Centre for Mathematical and Computational Modelling (ICM) at Warsaw University and partly at SPINLAB computing facility at Adam Mickiewicz University.

- 
- [1] S. Cahangirov, M. Topsakal, S. Ciraci, Phys. Rev. B 81, 195120 (2010).
- [2] B. Aufray, A. Kara, S. Vizzini, H. Oughaddou, C. Landri, B. Ealet, G. Le Lay, Appl. Phys. Lett. 96, 183102 (2010).
- [3] P. D. Padova, C. Quaresima, B. Olivieri, P. Perfetti, and G. Le. Lay, Appl. Phys. Lett. 98, 081909 (2011).
- [4] P. Vogt, P. De Padova, C. Quaresima, J. Avila, E. Frantzeskakis, M.C. Asensio, A. Resta, B. Ealet, and G. Le Lay, Phys. Rev. Lett. 108, 155501 (2012).
- [5] A. Kara, H. Enriquez, A. P. Seitsonen, L.C. Lew Yan Voon, S. Vizzini, B. Aufray, H. Oughaddou, Surf. Sci. Rep. 67, 1-18 (2012).
- [6] C.C. Liu, W. Feng and Y. Yao, Phys. Rev. Lett. 107, 076802 (2011).
- [7] N.D. Drummond, V. Zolyomi and V.I. Fal'ko, Phys. Rev. B85, 075423 (2012).
- [8] Z. Ni, Q. Liu, K. Tang, J. Zeng, J. Zhou, R. Qin, Z. Gao, D. Yu and J. Lu, Nano Lett. 12, 113 (2012).
- [9] W-F Tsai, C. Huang, T. Chang, H. Lin, H. Jeng and A. Bansil, Nature Comm. 4, 1500 (2013).
- [10] M. Miller, F.J. Owens, Chem. Phys. 381, 1 (2011); Y.-L. Song, Y. Zhang, J.-M. Zhang, D.-B. Lu, K.-W. Xu, Physica B 406, 69 (2011).
- [11] Ch. Zhang, Sh. Yan, J. Phys. Chem. C 116, 4163-4166 (2012).
- [12] J. Sivek, H. Sahin, B. Partoens, and F.M. Peeters, Phys. Rev. B87, 085444 (2013).
- [13] H. Sahin and F.M. Peeters, Phys. Rev. B87, 085423 (2013).
- [14] Y.C. Cheng, Z.Y. Zhu and U. Schwingenschlogl, Euro-Phys. Lett. 95, 17005 (2011).
- [15] C. Zhang and S. Yan, J. Phys. Chem. C 116, 4163 (2012).
- [16] N. Lu, Z.Y. Li, and J.L. Yang, J. Phys. Chem. C 113, 16741 (2009).
- [17] X-Q Wang, H-D Li and J-T Wang, Phys. Chem. Chem. Phys. 14, 3031 (2012).
- [18] X. Chen and J. Ni, Chem. Phys. Lett. 555, 173 (2013).
- [19] Y. Wang and Y. Ding, Solid State Comm. 155, 6 (2013).
- [20] Q.-X. Pei, Y.-W. Zhang, Z.-D. Sha and V. B. Shenoy, J. Appl. Phys. 114, 033526 (2013).
- [21] L. Pan, H. J. Liu, X. J. Tan, H. Y. Lv, J. Shi, X. F. Tang, G. Zheng, Phys. Chem. Chem. Phys., 14, 13588-13593 (2012).
- [22] K. Zberecki, M. Wierzbicki, J. Barnaś, R. Swirkowicz, Phys. Rev. B 88, 115404 (2013).
- [23] J. Kang, F. Wu, J. Li, Appl. Phys. Lett. 100, 233122 (2012).
- [24] Ch. Xu, G. Luo, Q. Liu, J. Zheng, Z. Zhang, S. Nagase, Z. Gao, J. Lu, Nanoscale, 4, 3111 (2012).
- [25] Y. Liang, V. Wang, H. Mizuseki and Y. Kawazoe, J. Phys. Cond. Matter, 24, 455302 (2012).
- [26] W. Wang, J. Zheng, Z. Ni, R. Fei, Q. Liu, R. Quhe, C. Xu, J. Zhou, Z. Gao and J. Lu, Nano 7, 1250037 (2012).
- [27] X-T An, Y-Y Zhang, J-J Liu, S-S Li, New J. Phys. 14, 083030 (2012).
- [28] Y. Ding and Y. Wang, J. Phys. Chem. C, 117, 18266 (2013).
- [29] F. Zheng, C. Zhang, S. Yan and F. Li, J. Mater. Chem. C, 1, 2735 (2013).
- [30] X-T An, Y-Y Zhang, J-J Liu, S-S Li, , arXiv:1305.3684v1
- [31] M. Walter, J. Walowski, V. Zbarsky, M. Mnzenberg, M. Schfers, D. Ebke, G. Reiss, A. Thomas, P. Peretzki, M. Seibt, J.S. Moodera, M. Czerner, M. Bachmann, Ch. Heiliger, Nature Mat. 10, 742 (2011).
- [32] N. Liebing, S. Serrano-Guisan, K. Rott, G. Reiss, J. Langer, B. Ocker, H.W. Schumacher, Phys. Rev. Lett. 107, 177201 (2011).
- [33] K. Uchida, S. Takahashi, K. Harii, J. Ieda, W. Koshibae, K. Ando, S. Maekawa, E. Saitoh, Nature 455, 778 (2008).
- [34] M. Wierzbicki, R. Swirkowicz, and J. Barnaś, Phys. Rev. B80, 195409 (2009).
- [35] D. Sanchez-Portal, P. Ordejon, E. Artacho, J. M. Soler, Int. J. Quantum Chem. 65, 453 (1997).
- [36] M. Brandbyge, J.-L. Mozos, P. Ordejon, J. Taylor, K. Stokbro, Phys. Rev. B 65, 165401 (2002).
- [37] Y.-W. Son, M. L. Cohen, S. G. Louie, Phys. Rev. Lett. 97, 216803 (2006).
- [38] D.M. Ceperley and B.J. Alder. Phys. Rev. Lett., 45, 566, (1980).
- [39] J.P. Perdew and A. Zunger. Phys. Rev. B, 23, 5048, (1981).
- [40] J.P. Perdew, K. Burke, and M. Ernzerhof. Phys. Rev. Lett., 77, 3865 (1996).

